14th International Symposium on Turbulence and Shear Flow Phenomena (TSFP14)
Heidelberg, Germany, July 28–31, 2026

TRANSITION TO THE ULTIMATE REGIME OF TURBULENT CONVECTION IN STRATIFIED INCLINED DUCT FLOW

Rundong Zhou
Physics of Fluids Department,
University of Twente,
7500 AE Enschede, Netherlands
rundong.zhou@utwente.nl

Adrien Lefauve
Grantham Institute - Climate Change and the Environment,
Imperial College London,
SW7 2AZ London, UK
Department of Civil and Environmental Engineering,
Imperial College London,
SW7 2BU London, UK
a.lefauve@imperial.ac.uk

Roberto Verzicco
Physics of Fluids Department,
University of Twente,
500 AE Enschede, Netherlands
Dipartimento di Ingegneria Industriale,
University of Rome 'Tor Vergata',
00133 Rome, Italy
Gran Sasso Science Institute,
67100 L'Aquila, Italy
verzicco@uniroma2.it

Detlef Lohse
Physics of Fluids Department,
University of Twente,
500 AE Enschede, Netherlands
Max Planck Institute for Dynamics and Self-Organization,
37077 Göttingen, Germany
d.lohse@utwente.nl

ABSTRACT

The stratified inclined duct (SID) provides a canonical setup for sustained, buoyancy-driven exchange flow between two reservoirs of different density, and emerges as a new paradigm in geophysical fluid dynamics. Yet, the flow dynamics remain unclear in the highly turbulent regime; laboratory experiments can access this regime but they lack resolution, while direct numerical simulations (DNS) at realistically high Prandtl number $\mathrm{Pr} = 7$ (for heat in water) have not achieved sufficiently high Reynolds numbers Re. We conduct three-dimensional DNS up to $\mathrm{Re} = 8000$ and observe the transition to the so-called ultimate regime of turbulent convection as evidenced by the Nusselt number scaling $\mathrm{Nu} \sim \mathrm{Ra}^{1/2}$, indicating substantially enhanced transport. At the transition the shear Reynolds number, a key parameter characterizing boundary layer (BL) dynamics, exceeds the threshold range of 420 for turbulent kinetic BLs with the emergence of logarithmic velocity profiles. The nature of the transition towards ultimate SID flow is non-normal-nonlinear, i.e., subcritical and hysteretic, as is typical for the transition to fully turbulent shear flows. Our work connects SID flow with the broader class of wall-bounded turbulent convection flows and gives insight into mixing properties in the vigorously turbulent regime encountered in oceanographic and industrial flows.

INTRODUCTION

Buoyancy-driven exchange flows occur in many natural and built environments when two large bodies of fluid at different densities are connected through a narrow channel. Such flows cause significant exchange of scalars (e.g., heat, salt, pollutants, nutrients) between the two reservoirs with minimal to no net volume transport (Wood, 1970; Wilkinson, 1986). They underpin key mixing and transport processes in oceanography and industrial flows. For example, the Mediterranean Sea depends on exchanges through the straits of Gibraltar and the Bosphorus (Deacon, 1971), coastal environments depend

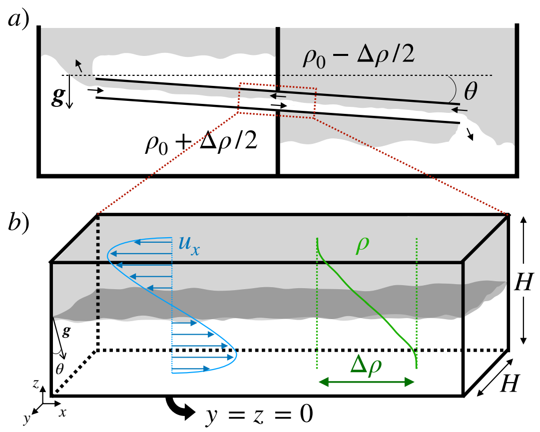

Figure 1. (a) Schematic illustration of the SID experiment. (b) Detail of the mid-duct region in the duct reference frame, showing typical vertical profiles of mean streamwise velocity (blue) and density (green).

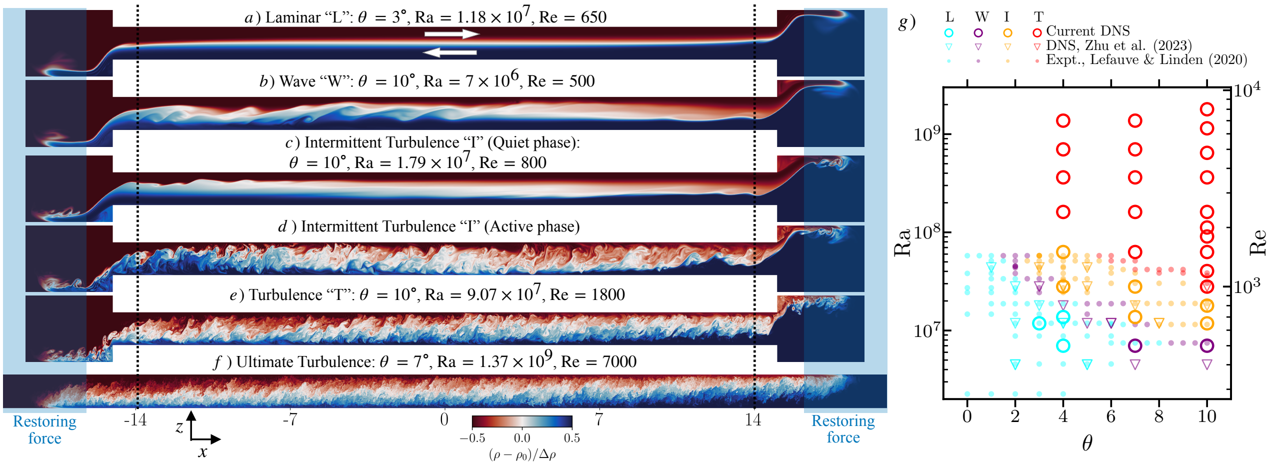

Figure 2. (a-f) Snapshots of the spanwise mid-plane density field ρ for increasingly turbulent flow regimes. The flow directions are indicated by arrows in (a). The z-axis is scaled up by 1.5. Simulations include artificial restoring forces applied in the blue regions. The quantities are averaged within $x/H \in [-14, 14]$ (black dashed lines) to eliminate edge effects. (g) Qualitative flow regime phase diagram illustrating the current DNS results alongside previous experimental (Lefauve & Linden, 2020) and numerical (Zhu *et al.*, 2023) data at $\mathrm{Pr} = 7$.

on estuarine transport processes (Fischer, 1976; MacCready *et al.*, 2018), and natural air ventilation in buildings and industrial safety scenarios depend on exchange between stratified air masses (Linden, 1999). Moreover, these flows are inherently stably stratified shear flows, ideal for studying shear instabilities and sustained stratified turbulence, a research lineage extending back to seminal works by Reynolds (1883) and Taylor (1931).

The stratified inclined duct (SID) experiment was developed by Meyer & Linden (2014) to study such buoyancy-driven exchange flows with sustained shear under well-controlled conditions, serving as a continuous realization of Thorpe (1968)'s seminal closed tilted-channel experiments. SID is schematically illustrated in fig. 1: two reservoirs are filled with liquids of different densities $\rho_0 \pm \Delta\rho/2$, connected via a long rectangular duct tilted at an angle θ from the horizontal in the laboratory frame. Once the duct is opened, a transient gravity current occurs, after which a sustained, buoyancy-driven, two-layer stratified exchange flow develops. SID flow has emerged as a novel paradigm in fluid mechanics for exploring the routes to stratified turbulence, exhibiting rich transitional and intermittent dynamics which have been well documented over the last decade, for a review, see Lefauve (2024). With increased driving, either through larger density differences $\Delta\rho/\rho_0$ or greater inclination θ, the flow typically transitions through four qualitatively distinct regimes—laminar, wave, intermittently turbulent, and fully turbulent.

The dimensionless Rayleigh number

$$\mathrm{Ra} \equiv \frac{g(\Delta\rho/\rho_0)H^3}{\nu\kappa} \tag{1}$$

quantifies the strength of the buoyancy driving, where H is the duct height and serves as the characteristic length scale, ν the kinematic viscosity, κ the thermal diffusivity, and g the gravitational acceleration. Ra serves as a primary control parameter along with the inclination θ. The hydraulic Reynolds number, sometimes used in the literature,

$$\mathrm{Re} \equiv \frac{\sqrt{g(\Delta\rho/\rho_0)H}(H/2)}{\nu} = \frac{1}{2}\mathrm{Ra}^{1/2}\,\mathrm{Pr}^{-1/2} \tag{2}$$

is an equivalent parameter to Ra in this work as we fix the Prandtl number, $\mathrm{Pr} \equiv \nu/\kappa = 7$, approximating heat in water around 20°C. For salt in water, the corresponding $\mathrm{Pr}_s \equiv \nu/D = 700$ (also called Schmidt number Sc), with D being the molecular diffusivity, is two orders of magnitude larger. The velocity scale is the free-fall velocity $U_0 \equiv \sqrt{g(\Delta\rho/\rho_0)H}$, the typical observed peak velocity, while the lengthscale is $H/2$ in Re Lefauve (2024). The regimes are visualized by the density field snapshots and classified by the phase diagram in fig. 2.

A key feature of SID flow is that its shear is generated exclusively by buoyancy, distinguishing it from canonical sheared convective flows that are typically driven mechanically (Blass *et al.*, 2020; Zhou *et al.*, 2017), or by external forcing mechanisms and imposed pressure gradients (Yerragolam *et al.*, 2024; Howland *et al.*, 2024). Additionally, it is bounded by no-slip sidewalls. These characteristics connect SID flow to other extensively studied canonical buoyancy-driven wall-bounded systems such as Rayleigh–Bénard (RB) convection (flow heated from below and cooled from above in an enclosed domain) (Ahlers *et al.*, 2009; Lohse & Shishkina, 2024), axially homogeneous RB convection, also known as convection in a vertical channel (CVC) (Schmidt *et al.*, 2012; Casting *et al.*, 2017), vertical convection (flow between two vertical heated and cooled plates) (Ng *et al.*, 2015; Ke *et al.*, 2023), and Taylor-Couette flow (flow between two coaxial co- or counter-rotating cylinders) (Dubrulle & Hersant, 2002; Grossmann *et al.*, 2016). In particular, for an extreme $\theta = 90°$, SID is a realization of CVC, where the heated/cooled plates of RB are replaced by reservoirs. For small θ, SID retains distinct features of a stably stratified, strongly sheared mean exchange flow. In spite of the recent interest, SID flow characteristics in the strongly turbulent regime have remained out of reach. Experiments at have reached $\mathrm{Re} = \mathscr{O}(10^4)$ at $\mathrm{Pr}_s = 700$ (Lefauve & Linden, 2020; Lefauve & Couchman, 2024) but measurements of the velocity and density fields have so far been restricted to $\mathrm{Re} = \mathscr{O}(10^3)$ (Lefauve & Linden, 2022*a*,*b*). Likewise, numerical simulations resolve the full flow fields but have also been restricted to $\mathrm{Re} = \mathscr{O}(10^3)$ at $\mathrm{Pr} = 7$ (Zhu *et al.*, 2023).

In this work, we overcome these limitations by directly simulating highly turbulent SID flow up to $\mathrm{Re} = 8000$, cor-

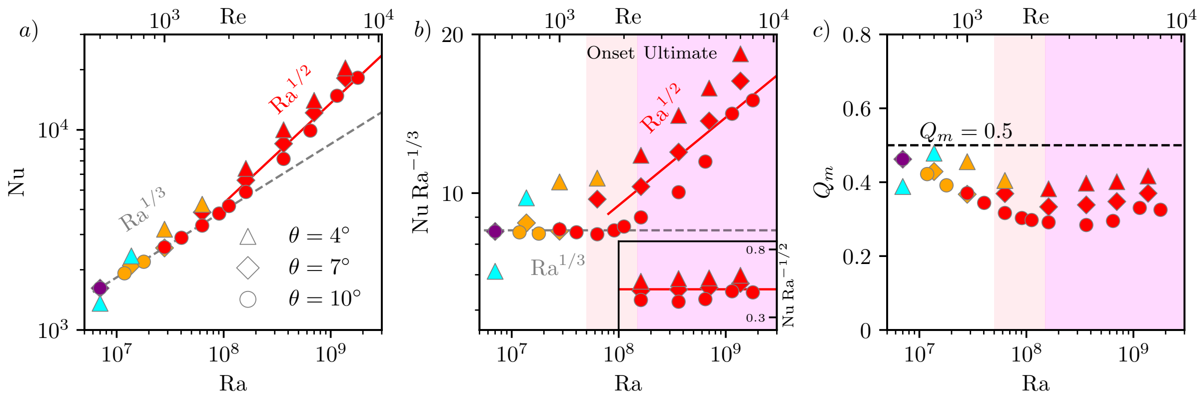

Figure 3. (a) Log-log plot of Nu against Ra. The fill color represents the flow regime as indicated in fig. 2g and the shape corresponds to the inclination. The slope for small Ra is consistent with Nu $\sim$ Ra$^{1/3}$ (dashed line). Scaling in the ultimate regime is guided by the red line Ra$^{1/2}$. (b) Same data as (a), but compensated by Ra$^{1/3}$. The inset shows the data in the ultimate regime compensated by Ra$^{1/2}$. (c) Hydraulic dimensionless mass flux Q_m against Ra, the vertical scale is linear. The dashed line marks the hydraulic limit $Q_m = 0.5$.

responding to Ra $= 1.8 \times 10^9$, see fig. 2g. Our main finding is a pronounced enhancement in mass transfer efficiency beyond a threshold of Ra $\approx 10^8$, with the scaling shifting from Nu $\sim$ Ra$^{1/3}$ to Nu $\sim$ Ra$^{1/2}$, consistent with the so-called ultimate regime of turbulent thermal convection first proposed by Kraichnan (1962) and found in homogeneous RB by Schmidt *et al.* (2012). This transition is concomitant with the development of turbulent boundary layers (BL), suggesting a novel turbulent channel configuration. These results provide the first observation of the ultimate regime in SID, and 3D numerical evidence of turbulent BLs in a purely buoyancy-driven system as previously found in vertical convection by Ke *et al.* (2023).

GLOBAL TRANSPORT

We begin by examining the primary observable of interest, the scalar transfer efficiency between the two reservoirs, quantified by the Nusselt number (the ratio of total transfer to purely conductive transfer; also called Sherwood number when referring to mass transfer):

$$\mathrm{Nu} \equiv \frac{\langle u_x(\rho-\rho_0)\rangle}{\kappa \Delta\rho / H} + 1, \tag{3}$$

where $\langle\cdot\rangle$ denotes the volume- and time-average over the duct region of volume $V = 28H^3$ between the black dashed lines in fig. 2(a-f). In fig. 3a, we present Nu as function of Ra in the range Ra $\in [6\times10^6, 2\times10^9]$ for three angles $\theta = \{4°, 7°, 10°\}$. Our results reveal two scaling regimes. For Ra $< 10^8$, the data are consistent with a scaling of Nu $\sim$ Ra$^{1/3}$, as expected for weakly driven thermal convection (Lohse & Shishkina, 2024). Beyond Ra $\approx 10^8$, the system undergoes a transition to the ultimate regime where the mass transfer efficiency follows the enhanced scaling Ra$^{1/2}$.

The transition is more apparent in fig. 3b, where Nu is compensated by Ra$^{1/3}$. In the low-Ra regime, data points scatter around the horizontal grey dashed line corresponding to Nu $\sim$ Ra$^{1/3}$, close to the effective scaling Nu $\sim$ Ra$^{0.3}$ reported by Pawar & Arakeri (2016) for weakly turbulent CVC. Here, turbulence is not fully developed (or transitional) and SID flow is affected by a family of linear instabilities as reported in Zhu *et al.* (2024), i.e., the first two points of $\theta = 4°$ deviate noticeably because the bulk flow structures are still laminar, as indicated by the fill color and flow visualization in fig. 2. The $\theta = 10°$ data follow the Nu $\sim$ Ra$^{1/3}$ scaling most closely, likely because the larger angle more closely resembles RB and CVC. Castaing *et al.* (2017) attributed this regime to the absence of Kolmogorov inertial range, yet scalar turbulence is already developed for Pr > 1. Near the onset (highlighted by orange shading in fig. 3b), the scaling departs from Ra$^{1/3}$, and in the ultimate regime (magenta shading), data align with the red line Nu $\sim$ Ra$^{1/2}$ for all three angles, highlighted in the inset. The ultimate regime reflects that the transport is independent of ν and κ. Under this assumption, the scaling is obtained by simple dimensional analysis (Kraichnan, 1962). We emphasize that the scaling is steeper than in the beginning of the ultimate regime of RB, where the logarithmic corrections from the turbulent thermal BLs yield an effective Nu $\sim$ Ra$^{0.38}$ scaling (Lohse & Shishkina, 2024). In contrast, in SID thermal BLs are eliminated by the reservoirs, and the entire channel is analogous to homogeneous RB flow.

We now turn our attention to the hydraulic dimensionless mass flux

$$Q_m \equiv \frac{2\langle u_x(\rho-\rho_0)\rangle}{U_0\,\Delta\rho} = \frac{2(\mathrm{Nu}-1)}{(\mathrm{Ra\,Pr})^{1/2}}, \tag{4}$$

a metric widely used in the hydraulics and stratified flow communities. According to classical hydraulic control theory for two-layer steady exchange flows, $Q_m \to 1/2$ in the inviscid limit Re, Ra $\to \infty$ (Armi, 1986; Dalziel, 1991). Figure 3c reveals a non-monotonic dependency of Q_m on Ra. In the low-Ra regime, Q_m approaches its maximal value of about 0.5 where the turbulence- or wave-driven exchange of the scalar across the density interface is minimal. As Ra increases, the flow becomes more turbulent and mixed, and Q_m decreases. It eventually plateaus in the ultimate regime towards a constant well below 0.5. Similar behavior has been documented in SID experiments with salt ($\mathrm{Pr}_s \approx 700$), where our and their Re are comparable, but Lefauve & Linden (2020)'s Ra $\approx 10^9$ – 10^{11} are two orders of magnitude higher than ours. In those experiments, Q_m converges to a larger asymptotic value close to 0.5 (see their fig. 6). Our data suggest a slight logarithmic uptrend in the ultimate regime, possibly hinting at $Q_m \to 0.5$ as Ra $\to \infty$. On the other hand, the Nu $\sim$ Ra$^{1/2}$ scaling is an upper bound for turbulent convection at finite Pr, implying that Q_m

is independent of Ra in the ultimate regime. Further investigation into the asymptotic behavior at large Ra and Re, as well as the influence of Pr would be valuable to better understand the (dis)similarities between SID flow and the broader class of wall-bounded turbulent convection.

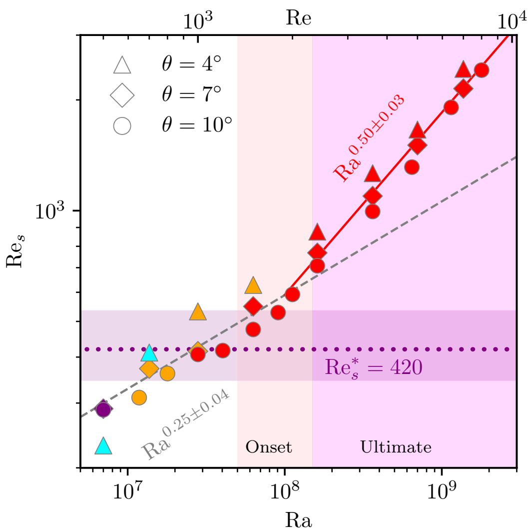

Figure 4. Log-log plot of shear Reynolds number Re_s against Ra. The purple horizontal dotted line and strip mark $\mathrm{Re}_s^* = 420$ around which the laminar BLs are expected to become turbulent, emphasizing the subcritical nature of the transition, which occurs over a range of Re_s. The fitted slopes match the expected $\mathrm{Re}_s \sim \mathrm{Ra}^{1/4}$ (dashed) for laminar BL and $\mathrm{Re}_s \sim \mathrm{Ra}^{1/2}$ (red solid) for turbulent BL.

SHEAR REYNOLDS NUMBER

The key parameter to characterize the transition of kinetic BL structure is the shear Reynolds number

$$\mathrm{Re}_s \equiv \frac{\max\langle u_x\rangle_{x,y,t}\,\delta^*}{\nu}, \tag{5}$$

based on the displacement BL thickness $\delta^* = \int_0^{z_{\max}} \left(1 - \frac{\langle u_x\rangle_{x,y,t}(z)}{\max\langle u_x\rangle_{x,y,t}}\right) \mathrm{d}z$ (Landau & Lifshitz, 1987), where $z_{\max}$ corresponds to the location of $\max\langle u_x\rangle_{x,y,t}$, associated with the BLs on top and bottom walls. In fig. 4, we plot Re_s as a function of Ra. In the low-Ra regime, we find that the measured slope $\mathrm{Re}_s \sim \mathrm{Ra}^{0.25} \sim \mathrm{Re}^{0.5}$, matches with the expected scaling based on the laminar BL thickness $\delta^*/H \sim \mathrm{Ra}^{-1/4} \sim \mathrm{Re}^{-1/2}$. In the ultimate regime, the scaling shifts to $\mathrm{Re}_s \sim \mathrm{Ra}^{1/2} \sim \mathrm{Re}$ for turbulent BLs. Landau & Lifshitz (1987) reported the estimate of $\mathrm{Re}_s^* \approx 420$ for the range of the transition to a turbulent BL (a detailed discussion can be found in Lohse & Shishkina (2024)). We observe that indeed $\mathrm{Re}_s > 420$ coincides with the onset region (highlighted in orange) where the Nu scaling changes (figs. 3a and 3b). This suggests that the transition to ultimate turbulence may be caused by changes in the BLs, although a coincidence cannot be ruled out.

TURBULENT BOUNDARY LAYERS AND STREAMWISE VELOCITY PROFILES

A hallmark feature of a turbulent BL is the log-law of the wall. We plot the averaged streamwise velocity profiles near $z = 0$ (bottom wall) at $y = H/2$ (spanwise mid-plane) in fig. 5a. The profiles are shown in the wall-normal units with $u^+ \equiv \langle u_x\rangle_{x,t}/u_\tau$, where $u_\tau = \sqrt{\nu\partial_z\langle u_x\rangle_{x,t}|_{z=0}}$ is the friction velocity, and the spatial coordinates $z^+ \equiv z/\delta_\nu$, with $\delta_\nu = \nu/u_\tau$ being the viscous unit. The magenta curves mark the profiles near the ultimate transition where the BLs have just turned turbulent. At large Ra, we notice that the curves converge to the shape of canonical 3D wall turbulence, comprising the viscous linear sublayer and by the short logarithmic region $u^+ = (1/\kappa_\nu)\ln z^+ + B$ with $\kappa_\nu = 0.41$ agreeing with the von Kármán constant. The parameter B differs slightly for different θ. We note that the logarithmic regions are not fully developed even at our highest Ra, spanning only about half a decade in z^+. This is not surprising: in SID, the logarithmic region is immediately followed by a negative mean velocity gradient in the bulk, arising from the counter-directional nature of the exchange flows, rather than by the free-streaming wake region of canonical turbulent boundary layers. This likely suppresses the log-law from extending further into z^+.

To further appreciate the features in the BLs in different regimes, we plot snapshots of the streamwise velocity u_x near the buffer layer $z^+ \approx 12$. The laminar BL in fig. 5b exhibits an overall smooth profile, with disturbances being generated upstream and dissipated downstream. The turbulent BL in fig. 5c is qualitatively different, exhibiting meandering streaks across the entire duct. These streaks are another hallmark of turbulent BLs, well-documented in canonical turbulent BL literature (Smits *et al.*, 2011). In the zoom-in fig. 5d, we observe that the spanwise spacings of these streaks are around 100-200 viscous units, consistent with previous studies on wall turbulence (Kline *et al.*, 1967; Smits *et al.*, 2011).

NATURE OF THE TRANSITION

The non-normal-nonlinear nature of the transition is demonstrated in figure 6. We run two time-dependent realizations spanning the onset and ultimate range of $\mathrm{Ra} \approx 5.5\times10^7 – 2.5\times10^8$ ($\mathrm{Re} \approx 1400 – 3200$; see fig. 3b). Starting in the intermittent regime, the compensated transport $\mathrm{Nu}(t)/\sqrt{\mathrm{Ra}(t)\mathrm{Pr}}$ shows strong intermittency, with peaks during the quiet phase (fig. 2c) and valleys during the active phase (fig. 2d). As Ra is slowly increased towards $\approx 2.5\times10^8$ (black curve), the fluctuations decrease significantly, marking the entry into the ultimate regime. During the ramp down, however, the ultimate regime persists until a much lower $\mathrm{Ra} \approx 1.5\times10^8$, after which intermittency reappears. The second realization (grey) transitions at different Ra, and the up- and down-ramp thresholds also differ from each other. This realization-dependence and hysteresis reflect that there is no single sharp Ra for the ultimate regime, and thus that the transition is subcritical and hysteretic.

Linear stability analysis suggests SID flow becomes linearly unstable for $\mathrm{Re} < 650$, $\mathrm{Ra} < 1.2\times10^6$ as reported by Zhu *et al.* (2024), well below the observed turbulent BL and ultimate transition. This finding suggests that the nonlinear subcritical shear instability developed within the BLs is crucial to trigger ultimate turbulent convection in SID. This contrasts with homogeneous RB (Schmidt *et al.*, 2012), where no evidence of turbulent BLs on the lateral walls has been reported.

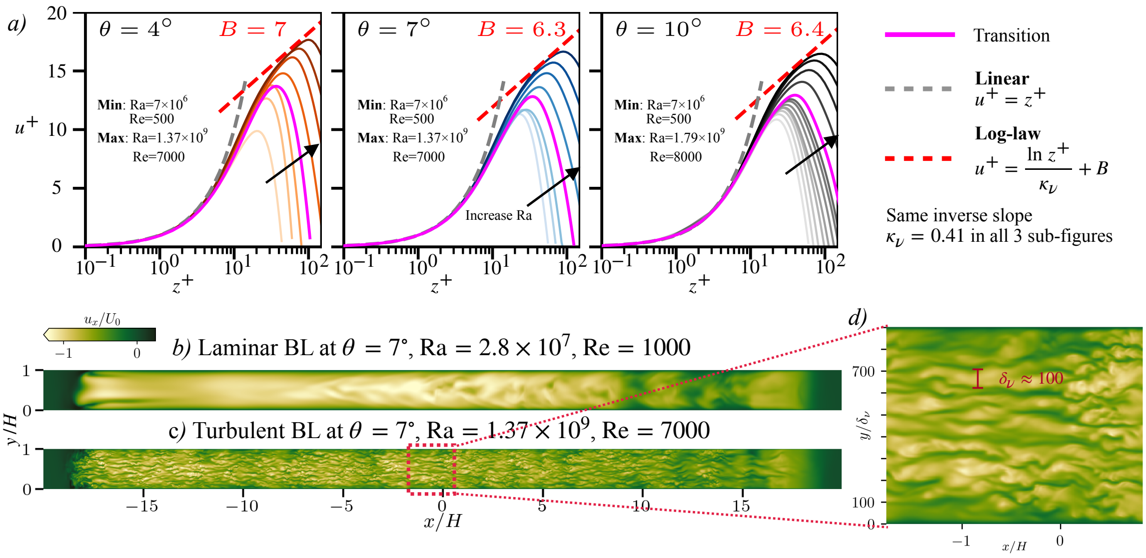

Figure 5. (a) Overall streamwise velocity $\langle u_x|_{y=H/2}\rangle_{x,t}(z)$ profiles in wall-normal units. Deeper colors represent higher Ra. The dashed lines correspond to the canonical 3D wall-bounded turbulence profile: (grey) the linear viscous sublayer, and (red) the log-law with inverse slope $\kappa_\nu = 0.41$ and B varies slightly for different θ. (b) Flow visualization (bottom view) of streamwise velocity u_x at $z \approx 12\delta_\nu$ inside the BL before the transition, and (c) after the transition, zoomed in (d). The y-axes are scaled up by 2 in (b-d).

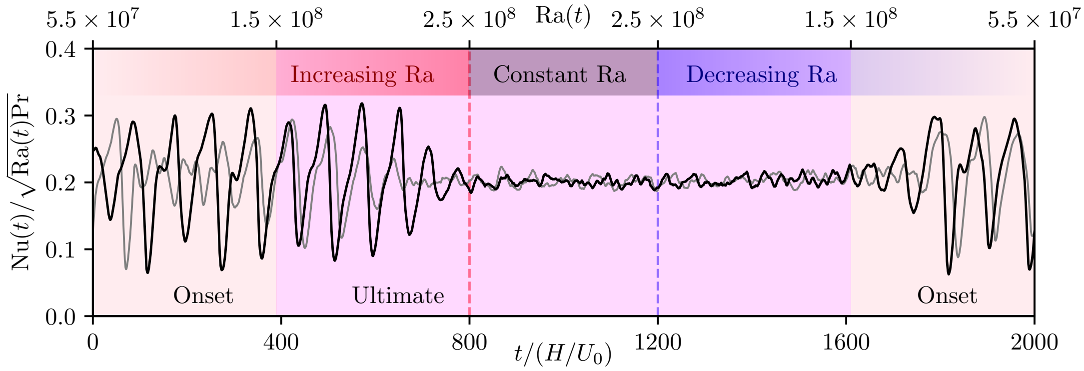

Figure 6. Hysteresis of the instantaneous Nu (compensated by $\sqrt{\mathrm{RaPr}}$) plotted against dimensionless time. The upper axis shows the imposed Ra(t): a slow linear ramp up, a constant hold, and an equally slow ramp down. Two independent realizations at $\theta = 4°$ are shown (black and grey). The up- and down-ramps span the transition Ra-range towards the ultimate SID regime, and the regime colors match fig. 3b

CONCLUSIONS AND OUTLOOK

In this work, we presented the 3D DNS of SID flow in the ultimate regime. The transition at Ra $\approx 10^8$ is marked by an enhancement in mass transfer efficiency to the asymptotic ultimate scaling of Nu $\sim$ Ra$^{1/2}$. We interpret this as the point where turbulent convection becomes the dominant driving mechanism, sustained by the formation of a streamwise uniform density gradient, analogous to the behavior observed in homogeneous RB. Simultaneously, the shear Reynolds number at the top and bottom walls exceeds $\mathrm{Re}_s^* \approx 420$, triggering turbulent BLs through a non-normal-nonlinear subcritical route. The Ra-range for the onset of the ultimate regime coincides with the turbulent BL transition, independently of the duct inclination θ, despite clear variations in global flow regimes with θ, supporting the interpretation that the transition is associated with the BLs. From a broader fluid dynamics perspective, SID flow offers a distinct internal wall shear flow configuration characterized by two extrema in the mean velocity profile, contrasting with canonical wall turbulence which exhibit either no extremum (plane Couette) or a single extremum (Poiseuille).

Many questions remain open. Although the asymptotic $Q_m = 1/2$ predicted by inviscid two-layer hydraulics coincides with the scaling Nu $\sim$ Ra$^{1/2}$, our results show that $Q_m < 0.5$ in the current range of Ra $\approx 10^7 - 10^9$. It remains unclear whether Q_m will remain below 0.5 indefinitely or eventually approach 0.5 as Ra $\to \infty$. Furthermore, our current interpretation is unlikely to hold for very small θ or in a horizontal duct ($\theta \approx 0°$), where the streamwise convective driving is weak or absent compared to horizontal hydrostatic pressure, even in the turbulent regime. Whether horizontal SID flow can exhibit the ultimate regime remains to be investigated.

Our results highlight universalities among various wall-bounded convective flows. Beyond fundamental fluid dynamics, our scaling laws for turbulent transport and energetics, including mixing efficiency, may help inform high-Re and high-Ra closure models in geophysics and engineering.

References

Ahlers, G., Grossmann, S. & Lohse, D. 2009 Heat transfer and large scale dynamics in turbulent Rayleigh–Bénard convection. *Rev. Mod. Phys.* **81**, 503–537.

Armi, L. 1986 The hydraulics of two flowing layers with different densities. *J. Fluid Mech.* **163**, 27–58.

Blass, Alexander, Zhu, Xiaojue, Verzicco, Roberto, Lohse, Detlef & Stevens, Richard J. A. M. 2020 Flow organization and heat transfer in turbulent wall sheared thermal convection. *J. Fluid Mech.* **897**, A22.

Castaing, B., Rusaouën, E., Salort, J. & Chillà, F. 2017 Turbulent heat transport regimes in a channel. *Physical Review Fluids* **2** (6), 062801.

Dalziel, S. B. 1991 Two-layer hydraulics: a functional approach. *J. Fluid Mech.* **223**, 135–163.

Deacon, M. 1971 *Scientists and the Sea 1650-1900, A Study of Marine Science*. London: Academic Press, London.

Dubrulle, B. & Hersant, F. 2002 Momentum transport and torque scaling in Taylor-Couette flow from an analogy with turbulent convection. *The European Physical Journal B - Condensed Matter and Complex Systems* **26** (3), 379–386.

Fischer, Hugo B. 1976 Mixing and Dispersion in Estuaries. *Ann. Rev. Fluid Mech.* **8** (1), 107–133.

Grossmann, S., Lohse, D. & Sun, C. 2016 High–Reynolds number Taylor–Couette turbulence. *Annu. Rev. Fluid Mech.* **48**, 53–80.

Howland, Christopher J., Yerragolam, Guru Sreevanshu, Verzicco, Roberto & Lohse, Detlef 2024 Turbulent mixed convection in vertical and horizontal channels. *Journal of Fluid Mechanics* **998**, A48.

Ke, Junhao, Williamson, N., Armfield, S. W. & Komiya, A. 2023 The turbulence development of a vertical natural convection boundary layer. *Journal of Fluid Mechanics* **964**, A24.

Kline, S. J., Reynolds, W. C., Schraub, F. A. & Runstadler, P. W. 1967 The structure of turbulent boundary layers. *Journal of Fluid Mechanics* **30** (4), 741–773.

Kraichnan, Robert H. 1962 Turbulent Thermal Convection at Arbitrary Prandtl Number. *The Physics of Fluids* **5** (11), 1374–1389.

Landau, L. D. & Lifshitz, E. M. 1987 *Fluid Mechanics*, 2nd edn., *Course of Theoretical Physics*, vol. 6. Exeter: Butterworth Heinemann.

Lefauve, Adrien 2024 Geophysical stratified turbulence and mixing in the laboratory. *Comptes Rendus. Physique* **25** (S3), 479–507.

Lefauve, Adrien & Couchman, Miles M. P. 2024 Data-driven classification of sheared stratified turbulence from experimental shadowgraphs. *Physical Review Fluids* **9** (3), 034603.

Lefauve, Adrien & Linden, P. F. 2020 Buoyancy-driven exchange flows in inclined ducts. *Journal of Fluid Mechanics* **893**, A2.

Lefauve, Adrien & Linden, P. F. 2022*a* Experimental properties of continuously forced, shear-driven, stratified turbulence. Part 1. Mean flows, self-organisation, turbulent fractions. *Journal of Fluid Mechanics* **937**, A34.

Lefauve, Adrien & Linden, P. F. 2022*b* Experimental properties of continuously forced, shear-driven, stratified turbulence. Part 2. Energetics, anisotropy, parameterisation. *Journal of Fluid Mechanics* **937**, A35.

Linden, P. F. 1999 The fluid mechanics of natural ventilation. *Ann. Rev. Fluid Mech.* **31**, 201–238.

Lohse, Detlef & Shishkina, Olga 2024 Ultimate Rayleigh-Bénard turbulence. *Reviews of Modern Physics* **96** (3), 035001.

MacCready, Parker, Geyer, W. Rockwell & Burchard, Hans 2018 Estuarine Exchange Flow Is Related to Mixing through the Salinity Variance Budget. *J. Phys. Oceanogr.* **48** (6), 1375–1384.

Meyer, C. R. & Linden, P. F. 2014 Stratified shear flow: experiments in an inclined duct. *J. Fluid Mech.* **753**, 242–253.

Ng, C. S., Ooi, A., Lohse, D. & Chung, D. 2015 Vertical natural convection: Application of the unifying theory of thermal convection. *J. Fluid Mech.* **764**, 0349–361.

Pawar, Shashikant S. & Arakeri, Jaywant H. 2016 Two regimes of flux scaling in axially homogeneous turbulent convection in vertical tube. *Physical Review Fluids* **1** (4), 042401.

Reynolds, O. 1883 An experimental investigation of the circumstances which determine whether the motion of water shall be direct or sinuous, and of the law of resistance in parallel channels. *Phil. Trans. Roy. Soc.* **174**, 935–982.

Schmidt, Laura E., Calzavarini, Enrico, Lohse, Detlef, Toschi, Federico & Verzicco, Roberto 2012 Axially homogeneous Rayleigh–Bénard convection in a cylindrical cell. *Journal of Fluid Mechanics* **691**, 52–68.

Smits, Alexander J., McKeon, Beverley J. & Marusic, Ivan 2011 High–Reynolds Number Wall Turbulence. *Annual Review of Fluid Mechanics* **43** (Volume 43, 2011), 353–375.

Taylor, G. I. 1931 Effect of Variation in Density on the Stability of Superposed Streams of Fluid. *Proc. Roy. Soc. A* **132** (820), 499.

Thorpe, S. A. 1968 A method of producing a shear flow in a stratified fluid. *Journal of Fluid Mechanics* **32** (4), 693–704.

Wilkinson, D. L. 1986 Buoyancy driven exchange flow in a horizontal pipe. *Journal of Engineering Mechanics* **112** (5), 485–497.

Wood, I. R. 1970 A lock exchange flow. *J. Fluid Mech.* **42** (04), 671–687.

Yerragolam, Guru Sreevanshu, Howland, Christopher J., Stevens, Richard J. A. M., Verzicco, Roberto, Shishkina, Olga & Lohse, Detlef 2024 Scaling relations for heat and momentum transport in sheared Rayleigh–Bénard convection. *Journal of Fluid Mechanics* **1000**, A74.

Zhou, Q., Taylor, J. R. & Caulfield, C. P. 2017 Self-similar mixing in stratified plane Couette flow for varying Prandtl number. *J. Fluid Mech.* **820**, 86–120.

Zhu, Lu, Atoufi, Amir, Lefauve, Adrien, Kerswell, Rich R. & Linden, P. F. 2024 Long-wave instabilities of sloping stratified exchange flows. *Journal of Fluid Mechanics* **983**, A12.

Zhu, Lu, Atoufi, Amir, Lefauve, Adrien, Taylor, John R., Kerswell, Rich R., Dalziel, Stuart B., Lawrence, Gregory A. & Linden, P. F. 2023 Stratified inclined duct: direct numerical simulations. *Journal of Fluid Mechanics* **969**, A20.